SANDIA REPORT
SAND2008-7852
Unlimited Release
Printed January 2009

Graphite Oxidation Modeling For Application in MELCOR

Fred Gelbard

Prepared by
Sandia National Laboratories
Albuquerque, New Mexico 87185 and Livermore, California 94550

Sandia is a multiprogram laboratory operated by Sandia Corporation,
a Lockheed Martin Company, for the United States Department of Energy's
National Nuclear Security Administration under Contract DE-AC04-94AL85000.

Issued by Sandia National Laboratories, operated for the United States Department of Energy by Sandia Corporation.

Available to DOE and DOE contractors from
U.S. Department of Energy
Office of Scientific and Technical Information
P.O. Box 62
Oak Ridge, TN 37831

Telephone: (865) 576-8401
Facsimile: (865) 576-5728
E-Mail: reports@adonis.osti.gov
Online ordering: http://www.osti.gov/bridge

Available to the public from
U.S. Department of Commerce
National Technical Information Service
5285 Port Royal Rd.
Springfield, VA 22161

Telephone: (800) 553-6847
Facsimile: (703) 605-6900
E-Mail: orders@ntis.fedworld.gov
Online order: http://www.ntis.gov/help/ordermethods.asp?loc=7-4-0#online

SAND2008-7852
Unlimited Release
Printed January 2009

Graphite Oxidation Modeling For Application in MELCOR

Fred Gelbard
fgelbar@sandia.gov
Sandia National Laboratories
P.O. Box 5800
Albuquerque, NM 87185-0748

Abstract

The Arrhenius parameters for graphite oxidation in air are reviewed and compared. One-dimensional models of graphite oxidation coupled with mass transfer of oxidant are presented in dimensionless form for rectangular and spherical geometries. A single dimensionless group is shown to encapsulate the coupled phenomena, and is used to determine the effective reaction rate when mass transfer can impede the oxidation process. For integer reaction-order kinetics, analytical expressions are presented for the effective reaction rate. For noninteger reaction orders, a numerical solution is developed and compared to data for oxidation of a graphite sphere in air. Very good agreement is obtained with the data without any adjustable parameters. An analytical model for surface burn-off is also presented, and results from the model are within an order of magnitude of the measurements of burn-off in air and in steam.

TABLE OF CONTENTS

1. INTRODUCTION

For nuclear reactors with graphite moderators, a possibility exists under hypothetical accident conditions for graphite combustion to add significant heat to the system. To assess this possibility, in this work a review is given of the MELCOR model proposed to account for graphite combustion.

We begin by reviewing in Section 2 the available data for graphite oxidation kinetics. We show that the MELCOR model is in good agreement with available data. Next in Section 3 we present a steady model that is simplified to uncouple the mass and energy balances within the graphite. The dimensionless form of the mass balance for arbitrary-order reaction kinetics is presented in Sections 4 and 5 for rectangular and spherical coordinates, respectively. Analytical solutions are given for zeroth- and first-order kinetics and numerical solutions for fractional-order kinetics are given in Section 5. In all these cases we show that just one dimensionless group, that expresses the rate of reaction to the rate of diffusion, can be used to summarize the process of coupled reaction and mass transport within graphite. The effects of also including mass transfer of oxidant from the bulk to the exterior surface of the graphite are discussed in Section 6. Data for graphite ignition are given in Section 7. However, as discussed in Section 8, no data were found on aerosol formation during graphite oxidation. In Section 9 the kinetics model is extended to estimate surface burn-off rates. In Section 10 the results of model calculations for half-order reaction kinetics coupled with mass transfer within a graphite sphere and to a cylindrical rod are compared to data. There is remarkably good agreement without any adjustable parameters. We conclude in Section 11 that the MELCOR model agrees with the limited data available, but additional work is needed for a range of oxidizing conditions, and for complex graphite geometries.

2. INTRINSIC GRAPHITE OXIDATION RATE

The oxidation of carbon has been extensively studied because of the interest in understanding coal combustion (Makino and Law, 1990; Makino, 1990; Makino, et al.,1994; Chelliah, 1996; Chelliah et al., 1996; Chelliah and Miller, 1997; Makino et al., 1998; Bews et al., 2001). For zonal model applications a single Arrhenius expression is a viable approach for the oxidation rate of graphite, with the reaction order with respect to oxygen varying from zero at low temperatures (~400 K) to unity at high temperatures (~ 2500 K), with ½ suggested at 1000 K (Backreedy et al., 2001). The vast literature on coal combustion could potentially serve as a basis for modeling the details of graphite combustion. However, the differences between reactor grade graphite and the numerous coals are too significant to ignore. Therefore, we concentrate this work on combustion data for graphite.

To accommodate various models for graphite oxidation and provide a computationally succinct expression, the MELCOR default for the reaction rate with oxygen is given by

$$R_{ox} = \frac{k_1 P_{O_2}^{n_1}}{1 + k_2 P_{H_2}^{n_2} + k_3 P_{O_2}^{n_3}} \text{ (gms graphite reacted/gms graphite sec)}, \qquad (1)$$

and the oxidation rate with steam is given by

$$R_{ox,steam} = \frac{k_4 P_{H_2O}^{n_1}}{1 + k_5 P_{H_2}^{n_2} + k_6 P_{H_2O}^{n_3}} \text{ (gms graphite reacted/gms graphite sec)} \qquad (2)$$

where

$$k_i = K_i \exp\left(-\frac{E_i}{R_{gas} T}\right) \quad i = 1, 2, \ldots 6, \qquad (3)$$

T is the absolute temperature, R_{gas} is the ideal gas constant, and P_{O_2}, P_{H_2}, and P_{H_2O} are the partial pressures of oxygen, hydrogen, and steam, respectively. The values for the parameters in Eqs. (1), (2), and (3) are given in Table 1. We will now assess the adequacy of the MELCOR default expression for reaction with oxygen against available

data. Comparable data were not found in the literature for reactions of graphite with steam.

Table 1. MELCOR default reaction rate parameters for the oxidation of graphite.

i	K_i	E_i/R_{gas}	n_i
1	3.889×10^4 $atm^{-1/2}$ s^{-1}	20129 K	1/2
2	0	0	-
3	0	0	-
4	26.8 atm^{-1} s^{-1}	16455 K	1
5	3.42×10^{-10} $atm^{-1/2}$	30596 K	1/2
6	4.95×10^{-16} $atm^{-1/2}$	39905 K	1

An early data set of interest was reported by Schweitzer and Singer (1962). Their low temperature oxidation rate data are compared to the MELCOR defaults in Figure 1. According to Schweitzer and Singer the data used in Figure 1 represent values from 200 graphite samples. Plotted are the results for ten different geometries. Proceeding in Figure 1 from left to right the geometries are a cylinder, flat plate, cylinder, rectangular prism, cylinder, cylinder, cylinder, rectangular prism, cylinder, and a cube. The scale of the geometries is on the order of an inch. A vertical line depicts the range, and a dot is given at the midpoint of the measured reaction rate range. The original rate data are given in terms of g $cm^{-2}sec^{-1}$. To compare the data to the rate expression in Eq. (1), an effective density and surface area must be specified. Unfortunately, Schweitzer and Singer do not state if the surface area for reaction is that contained throughout the porous structure or just the exterior of the geometry. The calculations in Figure 1 are based on the exterior area of the geometry and as reported by Richards et al. (1987), a density of 1.77 g/cm^3. As can be seen from Figure 1, the correlation in MELCOR provides a reasonable estimate of the reaction rate, and also supports the assumption that the area used to report the reaction rate is based on the exterior surface area.

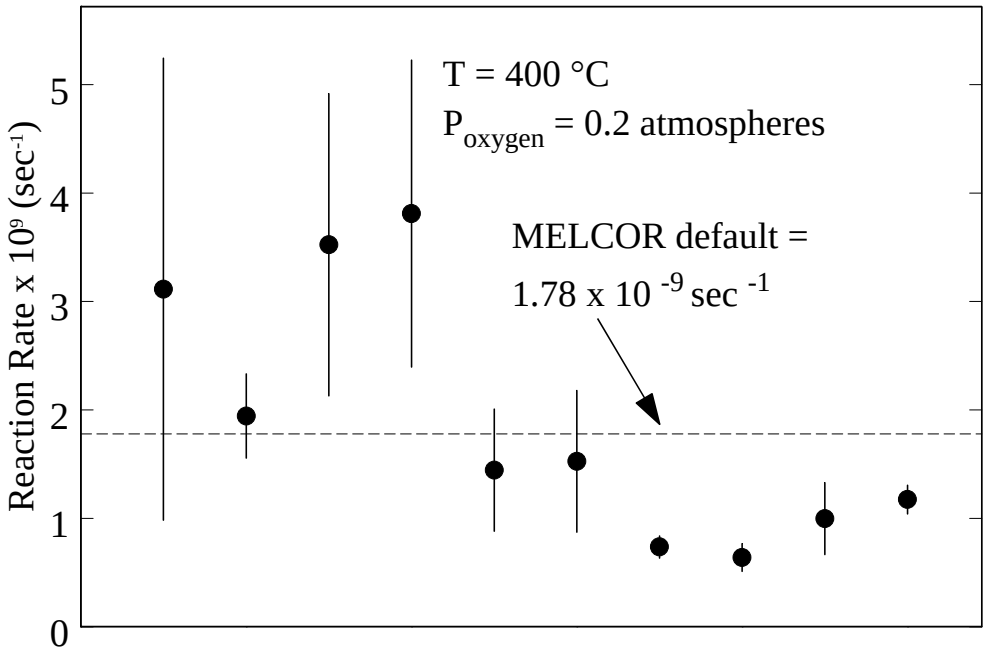

Figure 1. Comparison of MELCOR default reaction rate and data from Table I of Schweitzer and Singer, 1962. For the comparison we use $\rho_{graphite}$ = 1.77 g/cm^3 (Richards et al., 1987).

Another set of experiments of interest was reported by Froberg and Essenhigh (1978). In these experiments ½ inch-diameter graphite spheres were suspended inside a furnace and the mass was monitored as the graphite oxidized. The reported density and BET area were 1.65 g/cm^3 and 3 x 10^3 cm^2/g, respectively. At temperatures below 800 C the reported activation energy was 45 ± 1 kcal/mole. Thus for these experiments E/R = (45 ± 1 x 10^3)/1.9872 = 22645 ± 500 K. This activation energy is about 12% higher than the MELCOR default as given in Table 1.

Froberg and Essenhigh do not directly provide the reaction rate in a form that can be compared to the model used in MELCOR. However, from Fig. 7 of their work, the reaction rate is given as ~7 x 10^{-5} g cm^{-2} s^{-1} at 847 C. We use this data point because in their Fig. 3 this is the minimum temperature at which they provide the mass loss rate as ~3 x 10^{-5} g s^{-1} after the sphere has lost ~40% of its mass. They do not state whether the BET surface area or the exterior sphere area is the basis for their data in their Fig. 7. It is also unclear from their paper at exactly what point after some oxidation has occurred that the rate in their Fig. 7 is determined. Nonetheless, the area basis for their Fig. 7 may be deduced as follows. Assuming the sphere was originally half-inch in diameter and lost 40% of its mass, then (neglecting density changes with temperature) the sphere diameter was 0.422 inches when the mass loss rate was measured. Thus for this diameter the exterior surface area is 3.6 cm^2. By using the specific BET area of 3 x 10^3 cm^2 g^{-1} (and assuming it is independent of temperature), the BET area of the sphere is 3.2 x 10^3 cm^2. If the BET area is multiplied by the rate in their Fig. 7, the resulting mass loss rate is (3.2 x 10^3 cm^2)(7 x 10^{-5} g cm^{-2} s^{-1}) = 0.22 g s^{-1}. This is far too large compared to 3 x 10^{-5} g s^{-1}as reported in their Fig. 3 as the mass loss rate at 847 C. However, if the exterior area of the sphere is used, the resulting mass loss rate is 2.9 x 10^{-4} g s^{-1}. This is an order of magnitude larger than the mass loss rate in their Fig. 3, but is in far better agreement with the value given in their Fig. 7 than by using the BET area. Therefore we will assume that their area basis for calculating reaction rates is the exterior area of the sample, which is also the basis we used for the data reported by Schweitzer and Singer (1962). Some possible reasons why better agreement could not be obtained between Figs. 3 and 7 (in Froberg and Essenhigh) is that the effects of density changes and reactive area with temperature and oxidation are not included. In addition, visually determining values from a log-plot is not accurate.

Froberg and Essenhigh argue that the oxidation process is reaction-limited below 800 C. If we accept their arguments and an Arrhenius reaction rate description for graphite oxidation, then two parameters are needed, the activation energy and the reaction prefactor. As discussed above, Froberg and Essenhigh explicitly give the activation energy as 45 kcal/mole. The prefactor can be determined from the mass loss rate as a function of particle mass at a specific temperature. Unfortunately 847 C is the lowest temperature that the mass loss rate is given, and at this temperature the oxidation process is not totally reaction-limited. However, the prefactor can still be determined from their Fig. 7. In this Figure, in the temperature range of 800 K to 1050 K the eight data points fall exactly (to within visual perception) on a straight line fit with an activation energy of

45 kcal/mole. The rates are reported as being independent of oxygen concentration and gas flow rates up to 1 cm s^{-1}. From this Figure, at T = 800 K, the reaction rate is 3 x 10^{-8} g cm^{-2} s^{-1}. Thus at the initial stages of oxidation for a ½ inch diameter sphere, the reaction rate is given by,

$$k\exp\left(\frac{-22645}{800}\right)=\frac{\left(3x10^{-8}\,gcm^{-2}s^{-1}\right)\pi[(2.54)(0.5)cm]^2}{\frac{\pi}{6}\left(1.65gcm^{-3}\right)[(2.54)(0.5)cm]^3} \qquad (4)$$

Solving Eq. (4) results in k = 1.7 x 10^{5} s^{-1}. Thus the deduced Froberg and Essenhigh rate expression is given by

$$R_{ox,FE}=1.7\times10^{5}\exp\left[-\frac{22600}{T\,(^{\circ}K)}\right]\ (sec^{-1}). \qquad (5)$$

Bunnell et al. (1987) performed similar thermogravimetric experiments, but on cylindrical samples of TSX graphite (0.75 inch diameter, 1.5 inch long, and weighing ~19 grams), in air and obtained

$$R_{ox,BCT}=2.51\times10^{5}\exp\left[-\frac{23000}{T\,(^{\circ}K)}\right]\ (sec^{-1}). \qquad (6)$$

They also report that Dahl (1961) obtained a rate expression on CSF graphite as

$$R_{ox,D}=2.56\times10^{5}\exp\left[-\frac{22700}{T\,(^{\circ}K)}\right]\ (sec^{-1}). \qquad (7)$$

These experimental rate expressions can be compared to the default expression in MELCOR. For a partial pressure of oxygen of 0.2 atm, the default MELCOR reaction rate is

$R_{ox,MELCOR}$ = 3.889 x 10^{4} $atm^{-½}$ s^{-1}(0.2 atm)^{½} exp(-20129/T)

$$=1.7\times10^{4}\exp\left[-\frac{20129}{T\,(^{\circ}K)}\right]\ (sec^{-1}). \qquad (8)$$

The expressions in Eqs. (5) to (8) are compared in Figure 2. Considering that the experiments are based on different measurements and different graphites, there is fairly

good agreement among all the correlations. In particular, the agreement between the work of Bunnell et al. (1987) and our deduced rate from the work of Froberg and Essenhigh (1978) is excellent. At low temperatures, the MELCOR correlation seems to overestimate the reaction rate. However, as shown in Figure 1, for temperatures even lower than those in Figure 2, the default correlation in MELCOR is well within the measurements. Therefore, the low-temperature overestimate shown in Figure 2 by the MELCOR default correlation is not of concern.

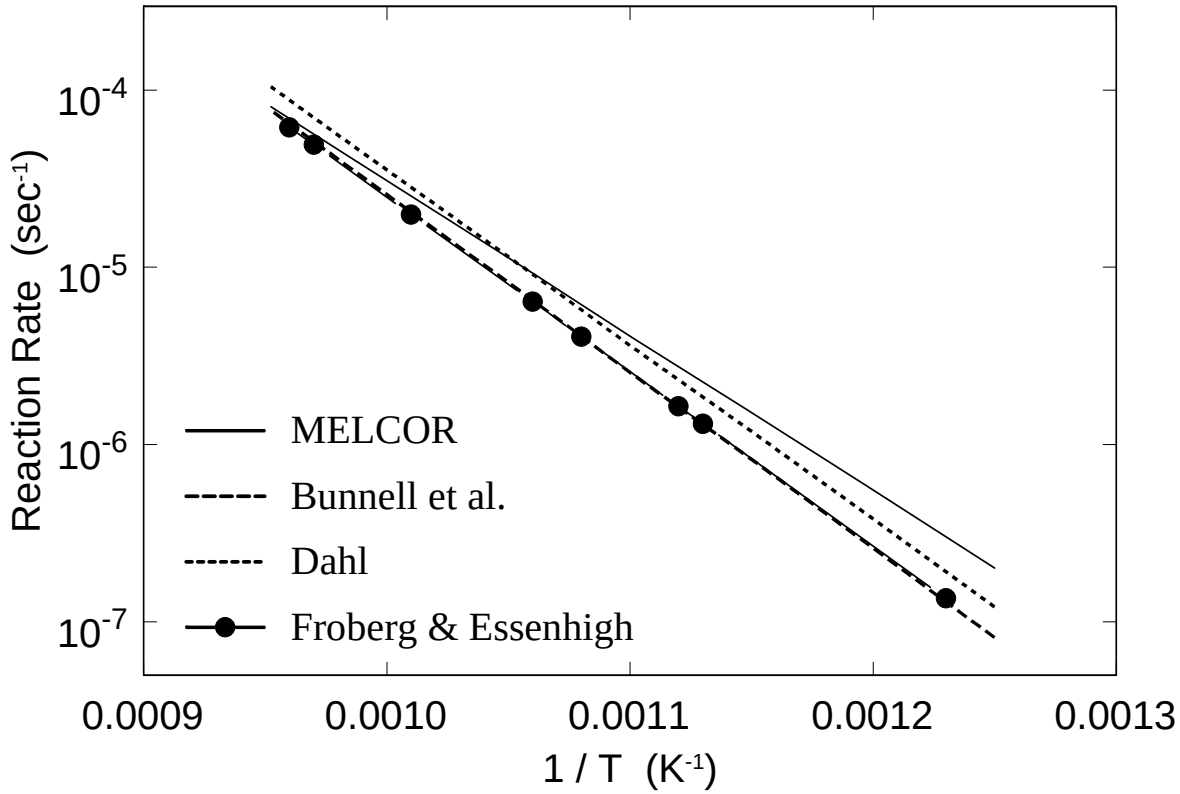

Figure 2. Comparison of MELCOR and experimental oxidation rates of graphite in air in the range 800 to 1050 K. The data points shown on the Froberg and Essenhigh line indicate the temperatures at which the reaction rates were deduced.

Some of the proposed expressions for the reaction rate at low temperatures are puzzling. Froberg and Essenhigh argue in their work that the dependency of the rate on the oxygen partial pressure is negligible if not zero. Although this was questioned at the time the work was presented, support for the low-order dependence on oxygen partial pressure at low temperatures seems to be the currently accepted description of the reaction (Backreddy et al., 2001). For example the expressions in Eq. (4) shows no dependency on the oxygen partial pressure. However, there clearly must be some dependency; otherwise, there could be oxidation without an oxidant, which is impossible. Furthermore, we show in this work that it is inconsistent to simultaneously claim that mass transfer limits the oxidation rate at high temperatures when the oxidant concentration plays no role in determining the oxidation rate. Possibly, the variation of oxygen partial pressure during the experiments was too small to observe significant changes in reaction rates. This would be consistent with the experiments and the proposed small reaction-order dependency at low temperatures suggested by Backreedy et al. (2001). The MELCOR approach to allow the reaction order to be an input variable provides the flexibility for both types of expressions. In the remainder of this work the

first- and zeroth-order reaction kinetics with respect to oxidant are used as limiting cases for analyzing the coupling of reaction and mass transport.

3. COUPLED PORE DIFFUSION AND GRAPHITE OXIDATION

The flux of oxidant through the pore space by diffusion can be given by,

$$N_{ox} = -\varepsilon D \frac{1}{R_{gas} T} \nabla P_{ox} \quad \text{(moles of oxidant } s^{-1} \text{ cm}^{-2}\text{)} \quad (9)$$

where D is the diffusivity, ε is the effective porosity of the material, and P_{ox} is the oxidant partial pressure. The effects of bulk flow within the pores on the flux of oxidant can be neglected if for each mole of oxidant (e.g. O_2), a mole of oxidized graphite (e.g. CO_2) is formed. In this case there is equimolar counter-diffusion, and hence no net bulk flow. Similarly, for low concentrations of oxidant at uniform pressure, the bulk flow effects can be neglected.

The rate of depletion of oxidant per unit volume is

$$\frac{F R_{ox} \rho_{graphite}}{M_{graphite}} \quad \text{(moles oxidant } s^{-1} \text{ cm}^{-3}\text{)} \quad (10)$$

where F is the number of moles of oxidant consumed per mole of graphite reacted, R_{ox} is the rate of oxidation of graphite, and $\rho_{graphite}$ and $M_{graphite}$ are the density and molecular weight of graphite, respectively. Combining Eqs. (9) and (10) into a steady state mass balance for the oxidant results in

$$\nabla \bullet N_{ox} = -\nabla \bullet \left[\varepsilon D \frac{1}{R_{gas} T} \nabla P_{ox} \right] = -\frac{F R_{ox} \rho_{graphite}}{M_{graphite}} . \quad (11)$$

In general, the mass balance given by Eq. (11) is coupled to an energy balance to determine the temperature as a function of spatial position. These coupled partial differential equations would require considerable computational resources for arbitrary three-dimensional geometries of graphite. Because this approach is not practical in a control volume model such as MELCOR, several approximations will be made to determine the overall effective reaction rate.

The diffusivity of gases is approximately proportional to the 1.5 power of temperature (Bird et al., p. 511, 1960). Therefore the ratio D/T is only weakly dependent on temperature and will be approximated as constant over the region of interest. Similarly, the product of the effective porosity and diffusivity is approximately constant. Thus the mass balance reduces to

$$\nabla \bullet \nabla P_{ox} = \frac{FR_{ox} R_{gas} T \rho_{graphite}}{\varepsilon D M_{graphite}}. \qquad (12)$$

If R_{ox} is either independent or linearly dependent of P_{ox}, (and not explicitly dependent on spatial position), then Eq. (12) is linear and therefore analytically solvable in separable geometries for separable and linear boundary conditions. We consider these two limits of R_{ox} dependency on P_{ox} because these seem to bound the reported dependency range (Backreedy et al., 2001). Numerical solutions will later be presented for fractional power dependencies of R_{ox} on P_{ox}. Thus in general R_{ox} will be given by

$$R_{ox} = AP_{ox}^{n} \qquad (13)$$

where A is a temperature-dependent function, and the reaction order n, will be in the range from 0 to 1. Because Eq. (12) is second order, two boundary conditions are needed. To obtain the first boundary condition we assume that there is sufficient flow past the graphite such that the oxidant partial pressure is constant on the exterior surface of the graphite. This provides the boundary condition that

$$P_{ox} = P_S \quad \text{(at the surface)}. \qquad (14)$$

Later P_S will be determined by additional analysis.

The second boundary condition is that the flux of oxidant is zero at a distance L within the graphite. If the geometry is symmetric such as oxidant diffusion into a sphere, a cylinder, or from both sides of a flat slab, then L is the distance from the exterior to the point, line, or plane of symmetry, respectively. The flux of oxidant may also be zero at an impermeable surface on one surface of the graphite. Thus the second boundary condition can be expressed mathematically as,

$$N_{ox} = -\varepsilon D \frac{1}{R_{gas} T} \nabla P_{ox} = 0 \quad \text{(at symmetric or impermeable boundary)}. \qquad (15)$$

We will now consider rectangular and spherical geometries for which exact explicit solutions can be obtained. The rectangular geometry is appropriate for oxidant transport through one face of a slab. The spherical geometry is useful for cases in which oxidant diffuses through all exterior surfaces.

4. ONE-DIMENSIONAL RECTANGULAR SOLUTION

Consider the specific case of one-dimensional rectangular coordinates for which the mass balance reduces to

$$\frac{d^2P_{ox}}{dx^2} = \frac{FAP_{ox}^{n}R_{gas}T\rho_{graphite}}{\varepsilon DM_{graphite}}. \quad (16)$$

The boundary conditions are

$$P_{ox} = P_s \quad (x = 0) \quad (17)$$

and

$$\frac{dP_{ox}}{dx} = 0 \quad (x = L, \text{ symmetric or impermeable boundary}). \quad (18)$$

Define the dimensionless partial pressure and dimensionless length as

$$\overline{P} = \frac{P_{ox}}{P_s} \quad \text{and} \quad (19)$$

$$\overline{x} = \frac{x}{L}, \quad (20)$$

respectively. Then in dimensionless form

$$\frac{d^2\overline{P}}{d\overline{x}^2} = \alpha^2\overline{P}^{n} \quad (21)$$

where the dimensionless group α^2 is given by,

$$\alpha^2 = \frac{FAP_s^{n-1}R_{gas}T\rho_{graphite}L^2}{\varepsilon DM_{graphite}}. \quad (22)$$

This dimensionless group expresses the ratio of the rate of reaction divided by the rate of pore diffusion. The dimensionless boundary conditions are

$$\overline{P} = 1 \quad (\overline{x} = 0) \quad (23)$$

and

$$\frac{d\bar{P}}{d\bar{x}} = 0 \qquad (\bar{x} = 1)\ . \qquad (24)$$

The solution for n = 1 has been reported previously (Cole and Rodriguez, 2000), and is given below in Table 2, which provides the exact solution for n = 1 and 0.

Table 2. One-dimensional rectangular analytical solutions.

Case	N	P_{ox}/P_s	$\frac{R_{gas}T}{\varepsilon D} N_{ox}\Big\|_{x=0} = -\frac{dP_{ox}}{dx}\Big\|_{x=0}$
1	1	$\frac{\exp[\alpha(1-\bar{x})] + \exp[-\alpha(1-\bar{x})]}{\exp(\alpha) + \exp(-\alpha)}$	$\frac{\alpha P_s \{\exp(\alpha) - \exp(-\alpha)\}}{L[\exp(\alpha) + \exp(-\alpha)]}$
2	0	$1 + \alpha^2\left(\frac{\bar{x}^2}{2} - \bar{x}\right)$ $(\alpha^2 \le 2)$	$\frac{\alpha^2 P_s}{L}$ $(\alpha^2 \le 2)$

$$\alpha = \sqrt{\frac{\rho_{graphite} F A P_s^{n-1} R_{gas} T L^2}{\varepsilon D M_{graphite}}}$$

The oxidant consumption is given by the flux of oxidant at x = 0, and is readily determined from the right-most column of Table 2. This provides the rate of oxidation per unit external area of exposed graphite, and hence the rate of heat release when multiplied by the heat of reaction per mole of oxidant consumed. For case 2 the reaction rate is independent of the oxidant partial pressure. Thus, the reaction may consume more oxidant than can be supplied by diffusion. The dimensionless group α^2 is therefore limited to at most 2, so as to avoid this unphysical situation. Otherwise the oxidant partial pressure within the graphite can be negative, which is clearly impossible.

For realistic oxidation mechanisms, pore diffusion can limit the reaction rate. Thus an effectiveness factor η, can be defined which is the ratio of oxidant consumption by pore diffusion followed by reaction, divided by the consumption rate by reaction without any diffusion limitations (Cole and Rodriguez, 2000). Thus,

$$0 \le \eta = \frac{SM_{graphite} N_{ox}\Big|_{x=0}}{V\rho_{graphite} FAP_s^n} \quad (25)$$

where V is the volume of graphite, and S is the exterior surface area through which oxidant diffuses into the graphite. Because V = SL, the dimensionless group α^2 can be used to express the effectiveness factor as

$$\eta = -\frac{L}{\alpha^2 P_s}\frac{dP_{ox}}{dx}\Big|_{x=0} . \quad (26)$$

The effectiveness factors for the two cases is given in Table 3 and plotted in Figure 3 for first-order kinetics. For case 2 the reaction rate is independent of the oxidant partial pressure, and the effectiveness factor is unity only for $\alpha^2 \le 2$. The dimensionless group α^2 increases as the reaction rate increases relative to the diffusion rate. As this occurs, there is less oxidant for reaction throughout the graphite, and thus from Figure 3 we see that as α^2 increases the effectiveness factor decreases.

Table 3. One-dimensional rectangular effectiveness factors.

Case	n	$\eta = \frac{SM_{graphite} N_{ox}\Big\|_{x=0}}{V\rho_{graphite} FAP_s^n}$
1	1	$\frac{1}{\alpha}\left(\frac{\exp(\alpha)-\exp(-\alpha)}{\exp(\alpha)+\exp(-\alpha)}\right)$
2	0	1

$$\alpha = \sqrt{\frac{\rho_{graphite} FAP_s^{n-1} R_{gas} TL^2}{\varepsilon DM_{graphite}}}$$

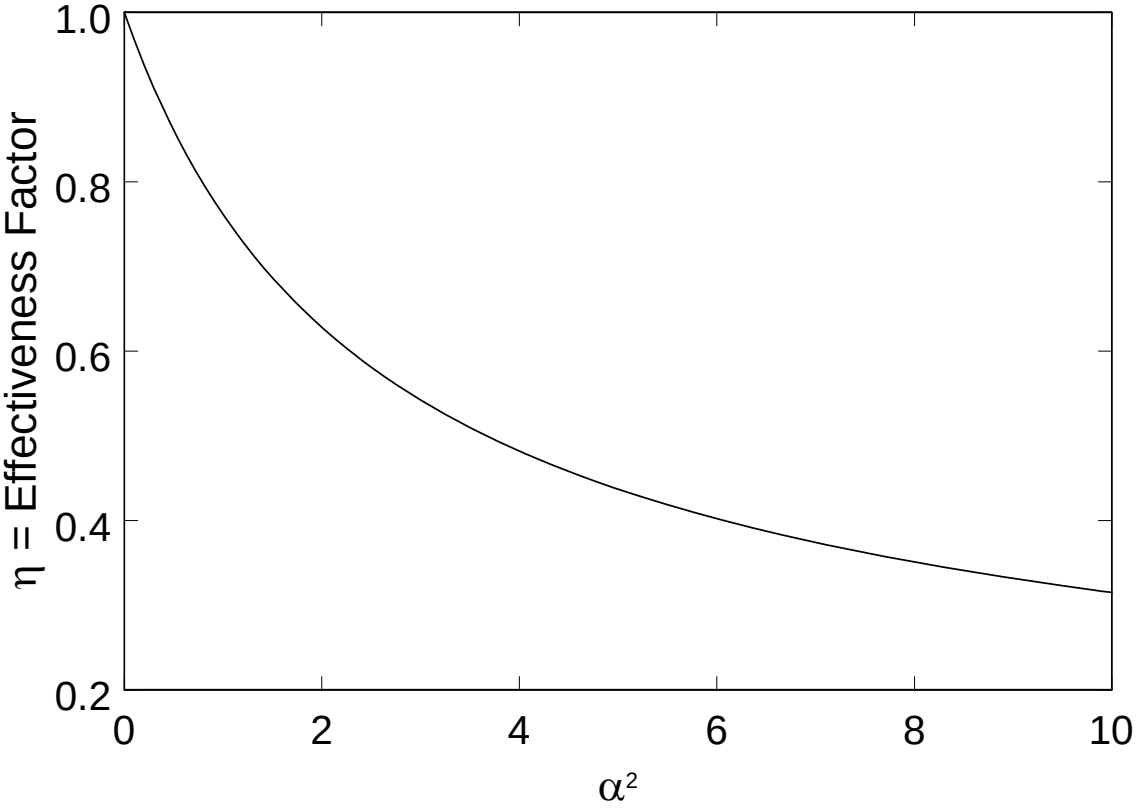

Figure 3. Effectiveness factor for one-dimensional rectangular coordinates and first-order kinetics.

5. ONE-DIMENSIONAL SPHERICAL SOLUTION

Consider now the specific case of one-dimensional spherical coordinates in the radial direction for which the mass balance reduces to

$$\frac{1}{r^2}\frac{d\left(r^2\frac{dP_{ox}}{dr}\right)}{dr}=\frac{FAP_{ox}^{n}R_{gas}T\rho_{graphite}}{\varepsilon DM_{graphite}} \qquad (0\le r\le R). \quad (27)$$

The boundary conditions are P_{ox} finite at r = 0, and $P_{ox} = P_s$ at r = R. The solutions for zeroth- and first-order kinetics are given in Table 5 as cases 3 and 4, respectively. (Case 4 with $R_{ox} = AP_{ox}$ is discussed in Bird et al., pp. 542-546, 1960.)

Define the dimensionless distance and the dimensionless partial pressure as $\bar{r} = r/R$ and $\bar{P} = P_{ox}/P_s$, respectively. Then the dimensionless form of the mass balance is

$$\bar{r}^2\frac{d^2\bar{P}}{d\bar{r}^2}+2\bar{r}\frac{d\bar{P}}{d\bar{r}}=\beta^2\bar{r}^2\bar{P}^n \qquad (28)$$

where the dimensionless group β^2 represents the ratio of the rate of reaction divided by the rate of pore diffusion and is given by

$$\beta^2=\frac{\rho_{graphite}FAP_s^{n-1}R_{gas}TR^2}{\varepsilon DM_{graphite}}. \quad (29)$$

The effectiveness factor is given by

$$\eta=-\frac{4\pi r^2M_{graphite}N_{ox}\Big|_{r=R}}{\frac{4}{3}\pi R^3\rho_{graphite}FAP_s^n}=-\frac{3M_{graphite}N_{ox}\Big|_{r=R}}{R\rho_{graphite}FAP_s^n}=\frac{3}{\beta^2}\frac{d\bar{P}}{d\bar{r}}\Big|_{\bar{r}=1} \qquad (30)$$

The exact solutions for the dimensionless oxidant partial pressure and the effectiveness factor are given in Table 4. Because N_{ox} is the flux in the positive radial direction, a minus sign has been included in Eq. (30) to obtain the flux of oxidant to the graphite. For nonspherical geometries, Bird et al., p. 545, 1960 suggests using an equivalent radius given by

$$R_{nonsp}=3\left(\frac{V}{S}\right). \qquad (31)$$

Thus, with Eq. (31) the expressions in Table 4 may also be used for irregularly shaped blocks of graphite.

Table 4. One-dimensional spherical solutions. (Note that N_{ox} is the molar flux of oxidant in the positive radial direction, which is away from the graphite sphere.)

Case	n	P_{ox}/P_s	$N_{ox}\big\vert_{r=R} = \left[-\frac{\varepsilon D \nabla P_{ox}}{R_{gas}T}\right]_{r=R}$	η
3	0	$1+\frac{\beta^2}{6}\left[\bar{r}^2-1\right]$ $(\beta^2 \le 6)$	$-\frac{\varepsilon D \beta^2 P_s}{3R_{gas}TR}$	1
4	1	$\frac{1}{\bar{r}}\left[\frac{\sinh(\bar{r}\beta)}{\sinh(\beta)}\right]$	$-\frac{\varepsilon D P_s(\beta\coth(\beta)-1)}{R_{gas}TR}$	$\frac{3}{\beta^2}(\beta\coth(\beta)-1)$

$$\beta = \sqrt{\frac{\rho_{graphite} F A P_s^{n-1} R_{gas} T R^2}{\varepsilon D M_{graphite}}}$$

For $R_{ox} = A P_s^n$ where n is between 0 and 1, Eq. (28) can be solved numerically using a Shooting Method (Press et al., 1992). We computed such solutions for n = 0.1, 0.3, and 0.5, and these are displayed in Figure 4. From this Figure we see that as β^2 increases, η decreases. This is expected because as the diffusion rate decreases relative to the reaction rate, less of the interior of the sphere is reacting. Hence, the effectiveness factor decreases. In the limit of reaction independent of the oxidant (i.e. n = 0), the effectiveness factor is unity regardless of the diffusion rate.

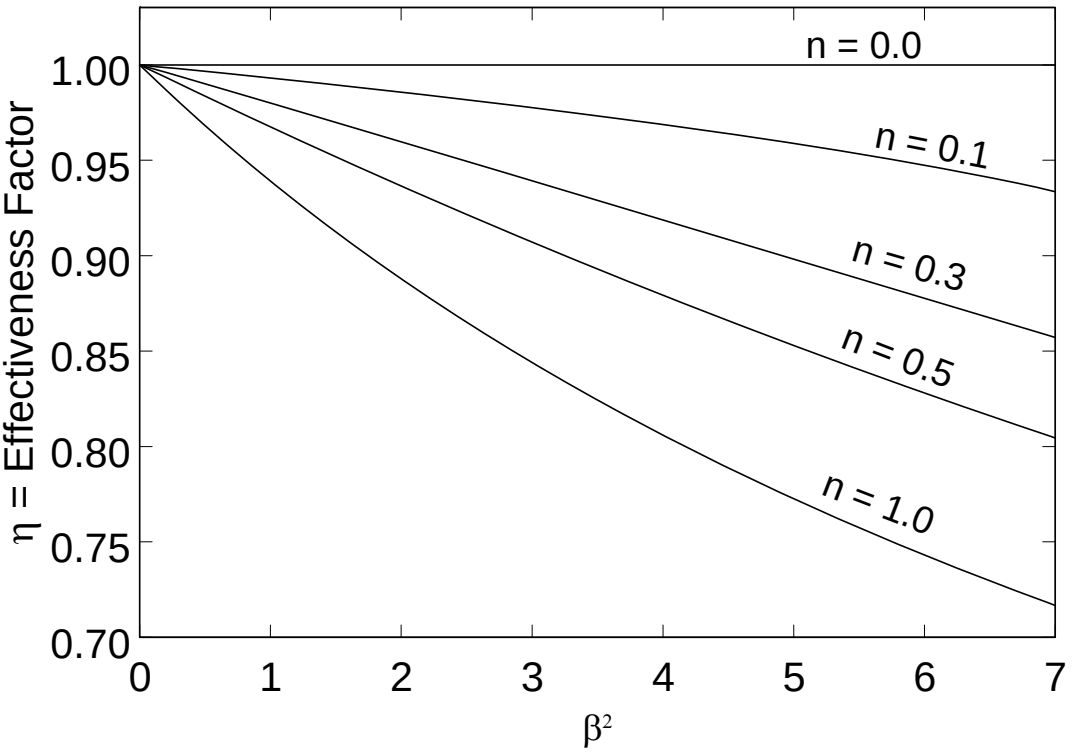

Figure 4. Effectiveness factor for n-th order reaction with pore diffusion in a sphere. Values of β^2 for which the effectiveness factor η, is close to 1 indicate that pore diffusion can be neglected and that the oxidant concentration is approximately equal to that at the outer surface of the sphere. An analytical expression is given in Table 4 for the curve when n =1.0.

6. COUPLED BULK DIFFUSION, PORE DIFFUSION, AND GRAPHITE OXIDATION

In addition to diffusion within graphite, there are also mass transfer considerations from the bulk fluid phase to the exterior surface of the graphite. This molar flux of oxidant towards the graphite can be given by

$$N_{ox}\Big|_{surface} = \frac{k_c (P_f - P_s)}{R_{gas} T_f} \qquad (32)$$

where k_c is the mass transfer coefficient, and T_f is the gas film temperature. The film temperature may be taken as the average of the bulk fluid temperature and the graphite temperature. Correlations are available to determine k_c for various geometries (Cole and Rodriguez, 2000). The surface partial pressure P_s, can be determined by equating the fluxes in Table 2 and Table 4 to that given in Eq. (32). Substituting this expression into Eq. (32) provides closed form expressions for the mass transfer rate for all four cases, and includes the effects of bulk diffusion to the surface, diffusion within the pore space, and either zeroth- or first-order chemical reaction. These expressions are given in Table 5. Then from Table 5 we can determine the conditions needed to neglect mass transfer from the bulk such that $P_s \cong P_f$. In addition, from Table 3 and Table 4 we can determine the conditions needed to neglect pore diffusion such that $P_{ox} \cong P_s$. The conditions when these approximations are valid are given in Table 6.

Table 5. Surface oxidant partial pressure including bulk diffusion, pore diffusion, and chemical reaction.

Case	n	Condition	P_s
1	1	$\left.\frac{dP_{ox}}{dx}\right\|_{x=L} = 0$	$\frac{P_f}{1+\frac{\varepsilon D \alpha T_f \tanh[\alpha]}{T k_c L}}$
2	0	$\left.\frac{dP_{ox}}{dx}\right\|_{x=L} = 0$	$P_f - \frac{\rho_{graphite} FALR_{gas} T_f}{M_{graphite} k_c}$
3	0	$P_{ox}\|_{r=0}$ finite	$P_f - \frac{\rho_{graphite} FARR_{gas} T_f}{3M_{graphite} k_c}$
4	1	$P_{ox}\|_{r=0}$ finite	$\frac{P_f}{1+\frac{\varepsilon D T_f (\beta \coth(\beta) - 1)}{T k_c R}}$

$$\alpha = \sqrt{\frac{\rho_{graphite} FAP_s^{n-1} R_{gas} TL^2}{\varepsilon D M_{graphite}}}, \quad \beta = \sqrt{\frac{\rho_{graphite} FAP_s^{n-1} R_{gas} TR^2}{\varepsilon D M_{graphite}}}$$

Table 6. Conditions needed to neglect bulk diffusion and therefore $P_S \cong P_f$, and to neglect pore diffusion, and therefore $P_{ox} \cong P_S$.

Case	$P_s \cong P_f$	$P_{ox} \cong P_s$
1	$\frac{\varepsilon D \alpha T_f \tanh[\alpha]}{Tk_c L} << 1$	$\frac{\tanh[\alpha]}{\alpha} \cong 1$
2	$\frac{\rho_{graphite} FALR_{gas} T_f}{M_{graphite} k_c P_f} << 1$	Always True
3	$\frac{\rho_{graphite} FARR_{gas} T_f}{3M_{graphite} k_c P_f} << 1$	Always True
4	$\frac{\varepsilon D T_f (\beta \coth(\beta) - 1)}{Tk_c R} << 1$	$\frac{3}{\beta^2}(\beta \coth[\beta] - 1) \cong 1$

$$\alpha = \sqrt{\frac{\rho_{graphite} FAP_s^{n-1} R_{gas} TL^2}{\varepsilon D M_{graphite}}}, \ \beta = \sqrt{\frac{\rho_{graphite} FAP_s^{n-1} R_{gas} TR^2}{\varepsilon D M_{graphite}}}$$

7. GRAPHITE IGNITION

Of concern for safety analysis is the ignition of the graphite that results in a flame. Much theoretical analysis and some experiments have been performed to address the phenomena for cylindrical graphite rods with steady gas flow towards the cylindrical surface (Makino and Law, 1990). This geometry is very convenient because the gas velocity field to a cylindrical surface can be determined analytically, thus enabling much theoretical analysis. Ignition was observed to be independent of the rod diameter in the diameter range tested of 0.5 to 2 cm, but dependent on the graphite surface temperature and flow velocities. There is considerable scatter in the data, and therefore we suggest a simple linear dependency of the ignition temperature with the logarithm of the free stream velocity gradient defined as 4V/d, where V is the free stream velocity and d is the rod diameter. From Fig. 8a of Makino and Law (1990), in air the ignition temperature is 1400 K for 4V/d = 50 sec^{-1}, and 1975 K for 4V/d = 1000 sec^{-1}. The ignition temperature decreases as the concentration of oxygen increases. For nearly pure oxygen, from Fig. 8b of Makino and Law (1990), the ignition temperature varies from 1350 K at 4V/d = 100 sec^{-1}, to 1700 K at 4V/d = 1000 sec^{-1}.

8. AEROSOL PARTICLE FORMATION

No data were found in the literature on aerosol particle formation from burning pure graphite. We assume that no graphite particles are aerosolized during the combustion process. However, one can expect that noncombustible impurities will result in aerosol particles. For MELCOR applications, we suggest assuming that the mass of impurities be placed in the smallest aerosol size bin.

9. SURFACE BURN-OFF

The graphite surface burn-off rate can be determined by assuming that the oxidation occurs in a thin surface layer of thickness δ. Then if the curvature effects are neglected in this region we have that the surface burn-off rate is given by

$$\dot{m} = R_{ox} \delta \rho_{graphite} \qquad (33)$$

Clearly, δ may not be larger than the sample of graphite. An empirical correlation for δ has been suggested by Wichner and Ball [p. A-9, 1997]. Their correlation is

$$\delta \text{ (millimeter)} = 9.368 \times 10^{-6} T^2 - 0.02859 T + 22.688 \qquad (34)$$

where T is the temperature in the range from 800 to 1500 K. We will test this model with experimental data in the next section.

10. COMPARISON WITH EXPERIMENTAL DATA

Froberg and Essenhigh (1978) report that at temperatures above about 1050 K, diffusion limited the consumption of graphite in their experiments. However, as we noted earlier, this conclusion is inconsistent with their reaction rate expression, which is independent of the oxygen partial pressure. If there is no dependency on the oxygen partial pressure, then there should not have been a reduction in rate due to mass transfer limitation. Nonetheless, we will now use their data to assess the MELCOR default expressions.

From Fig. 7 of Froberg and Essenhigh at an inverse temperature of 9×10^{-4} K^{-1} the ratio of the measured reaction rate to the rate calculated assuming no diffusion limitation is

$\eta = (6.5 \times 10^{-4})/(8.5 \times 10^{-4}) = 0.65$. (These values were obtained by the inaccurate process of reading numbers from a small log-plot.) The following values are reported for the experiment, $\rho_{graphite} = 1.65$ g cm^{-3}, R = 0.635 cm, and $\varepsilon = 0.18$. At this temperature, the rate data do not show a dependency on the air velocity past the sphere. Therefore, in agreement with the arguments given by Froberg and Essenhigh, we assume that there are negligible mass transfer limitations from the bulk to the surface of the graphite and thus $P_s = 0.2$ atm. In addition, $M_{graphite} = 12$ g $mole^{-1}$, $R_{gas} = 82.05$ atm cm^3 $mole^{-1}$ K^{-1}, F = 1.0, and $D = 0.206(T/298)^{1.823}$ cm^2 s^{-1}(Bird et al., 1960). From the MELCOR default parameters given in Table 1, $A = 3.889 \times 10^4$ $atm^{-1/2}$ $s^{-1}\exp(20129/T)$ and n = 0.5. Substituting these values into Eq. (29) results in

$$\beta^2 = \frac{\rho_{graphite} FAP_s^{n-1} R_{gas} TR^2}{\varepsilon D M_{graphite}} = 14.6 \quad (35)$$

Numerically integrating Eq. (28) for this value of β^2 and then substituting into Eq. (30) results in $\eta = 0.67$. This is remarkably very good agreement with the inferred measurement of $\eta = 0.65$, especially considering that there are no adjustable parameters in the analysis. However, because of the difficulty of visually obtaining accurate numbers from published plots, any agreement within 10 to 20 per cent should also be considered very good.

Froberg and Essenhigh reported that at high temperatures (above 1073 K), diffusion limited the oxidation rate. However, it is misleading to use temperature as the basis for determining when diffusion is important. It is not the temperature or the size of the graphite that determines whether mass transfer limits oxidation. Rather, as discussed above, it is whether the dimensionless group β^2 is high for a given reaction rate order. For a half-order reaction rate, i.e. n = ½, the effectiveness factor can be computed for oxidation of a graphite sphere in air. Plotted in Figure 5 is the effectiveness factor as a

function of spherical radius and temperature for graphite oxidation in air. Note that even at temperatures above 1100 K, if the radius is only 0.1 cm, then the effectiveness factor is essentially one. This indicates that pore diffusion does not limit the oxidation rate even at this high temperature.

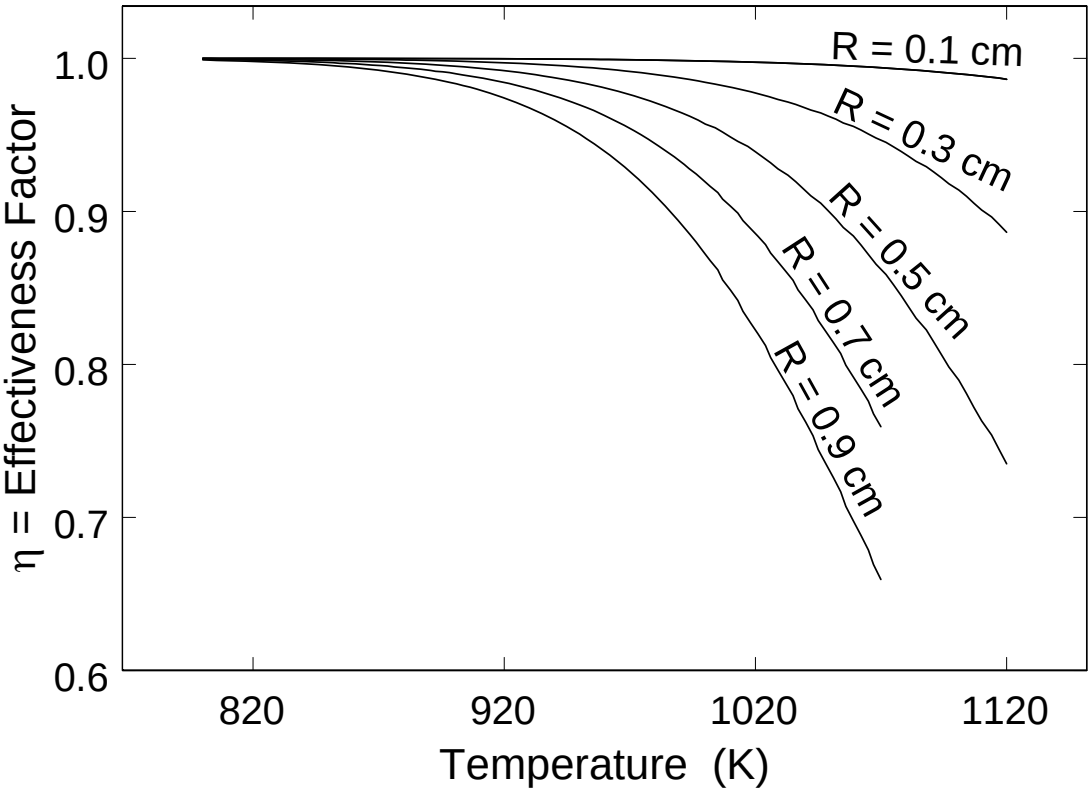

Figure 5. Effectiveness factor for graphite spheres or radius R oxidizing in air with half-order reaction kinetics.

Another series of experiments involved the oxidation of cylindrical graphite rods in steady flow towards the cylindrical surface [Makino, 1990; Makino and Law, 1990; Makino et al., 1994; Makino et al., 1998]. The rods in these experiments were 0.5 to 2 cm in diameter and 12 to 15 cm long, and were electrically Joule-heated by passing current through the rods. The surface temperature was determined by an optical pyrometer. From visual observations of the rod at the stagnation point at the center of the rod, the combustion rate was reported as

$$\dot{m} = \rho_{graphite} \ell / t \qquad (36)$$

where ℓ was the regression length of the graphite surface in the forward stagnation region, and t was the burning time [Makino, 1990]. To a good approximation, the regression length was found to be proportional to the burning time throughout the experiment. Although the authors refer to the data as the combustion rate, the data essentially provide a surface burn-off rate because the effects of oxidant diffusion and reaction within the graphite were not measured. Unfortunately, the graphite mass loss was not reported. The gas flow was characterized by the free stream velocity gradient defined as

$$a = 4V/d \quad (37)$$

where V is the free stream gas velocity towards the rod and d is the rod diameter.

There is considerable scatter in the data. Therefore, only typical values of the reported combustion rate at the upper and lower temperatures as given in Table 7 are used for comparison.

We can use the model given in Section 9 to analyze the experiments. At steady state the surface burn-off rate is equal to the flux of oxidant times the molecular weight of graphite and divided by F. (This of course assumes that no oxidant diffuses into the graphite.) Thus,

$$\dot{m} = \frac{k_c (P_f - P_s) M_{graphite}}{F R_{gas} T_f} \qquad (38)$$

where k_c is the local mass transfer coefficient. This coefficient can be determined from the local Sherwood number defined as

$$Sh_x \equiv \frac{x k_c}{D} \qquad (39)$$

where x is the distance from the stagnation line along the surface of the cylinder, and D is the diffusion coefficient. In the stagnation region the gas velocity is approximately Vx/d [Kakac et al., 1987, p. 2•57], where V is the free stream velocity. Thus the local Reynolds number is

$$Re_x = \frac{x^2 V\rho}{\mu d}. \quad (40)$$

Where μ and ρ are the viscosity and density, respectively of the gas stream. From the transport analogy, the Sherwood number can be determined from the correlation used for the Nusselt number for this geometry, and therefore

$$\frac{Sh_x}{Re_x^{1/2}} = \frac{\frac{k_c}{D}}{\sqrt{\frac{V\rho}{\mu d}}} \quad (41)$$

is correlated with the Schmidt number replacing the Prandtl number for stagnation flow [Kakac et al., 1987, p. 2•57]. The Schmidt number is defined as

$$Sc = \mu/(\rho D) \quad (42)$$

For Sc = 0.7, 0.8, 1.0, 5.0, and 10.0, then the dimensionless grouping in Eq. (41) is equal to 0.496, 0.523, 0.570, 1.043, and 1.344, respectively [Kakac et al., 1987, p. 2•57]. Thus, the dimensionless grouping in Eq. (41) is weakly dependent on the Schmidt number. At average film temperatures of 750 K and 1100 K, μ/ρ for air is 73.91×10^{-6} and 138.6×10^{-6} m^2/s, respectively [Eckert and Drake, p. 780, 1972]. The diffusion constant for oxygen through air is 1.533×10^{-5} m^2/s at 273.2 K [Eckert and Drake, p. 787, 1972], and varies as the 1.823 power of temperature [Bird et al, p. 505, 1960]. Thus at 750 K and 1100 K, Sc is 0.76 and 0.71, respectively. For these values of Sc the dimensionless grouping in Eq. (41) is approximately 0.5. Thus for analyzing the experiments the local mass transfer coefficient may be given by

$$k_c = \frac{D}{2}\sqrt{\frac{V\rho}{\mu d}}. \quad (43)$$

From Eqs. (33) and (38) a single equation can be given for the surface partial pressure of oxidant P_S as,

$$R_{ox}\delta\rho_{graphite} = \frac{k_c(P_f - P_s)M_{graphite}}{FR_{gas}T_f}. \quad (44)$$

In general, Eq. (44) is solved numerically for P_S. However, for $R_{ox} = A P_s^n$, where n = ½ or 1, P_S can be determined explicitly and then substituted into Eq. (33) to determine the burn-off rate for comparison with the experimental data. For n = 1,

$$P_s = \frac{P_f}{\frac{A\delta\rho_{graphite} FR_{gas} T_f}{k_c M_{graphite}} + 1} \qquad (n = 1) \quad (45)$$

and for n = ½,

$$P_s = P_f + \frac{1}{2}\left[\frac{A\delta\rho_{graphite} FR_{gas} T_f}{k_c M_{graphite}}\right]^2 \left[1 - \sqrt{1 + 4P_f \left\{\frac{k_c M_{graphite}}{A\delta\rho_{graphite} FR_{gas} T_f}\right\}^2}\right]. \quad (46)$$

For the experiment numbers 1 and 3 in Table 7 at T = 1200 K, the parameters are F = 1, n = ½, and $\delta = 1.87 \times 10^{-3}$ m. For the MELCOR default oxidation expression given in Eq. (1), $A = 3.889 \times 10^{4}$ atm$^{-½}$ s^{-1}exp(-20129/1200)[atm/1.01325×10^{5} Pa]^{½} = 6.3×10^{-6} Pa$^{-½}$ s^{-1}. For T_f = 750 K, $\mu/\rho = 73.91 \times 10^{-6}$ m^2/s, and $D = 9.7 \times 10^{-5}$ m^2/s. In addition, $\rho_{graphite} = 1.69 \times 10^{3}$ kg/m^3, constant R_{gas} = 8314.4 J K^{-1} kg-mole^{-1}, and $M_{graphite}$ = 12 kg/kg-mole. Then k_c is determined from Eqs. (43), and from Eq. (46), P_s can be determined and is given in Table 7. Substituting P_s into Eq. (33) results in the calculated mass burn-off rate that is given in Table 7. From this table for data sets 1 and 3, from columns 8 and 9 we see there is fairly good agreement, especially considering that no adjustable parameters are used in the analysis.

For experiment numbers 2 and 4 in Table 7 at T = 2000 K, the correlation for δ given in Eq. (33) is invalid. As an approximation we use $\delta = 8.7 \times 10^{-4}$ m, which corresponds to the smallest value of δ in Eq. (33), and is valid for T = 1526 K. For the MELCOR default oxidation expression given in Eq. (1), $A = 3.889 \times 10^{4}$ atm$^{-½}$ s^{-1}exp(-20129/2000)[atm/1.01325×10^{5} Pa]^{½} = 5.2×10^{-3} Pa$^{-½}$ s^{-1}. For T_f = 1100 K, $\mu/\rho = 138.6 \times 10^{-6}$ m^2/s, and $D = 1.9 \times 10^{-4}$ m^2/s. The calculated and measured burn-off rates for tests 2 and 4 are given in Table 7. The agreement is good for low flows, but is not good at the higher flow rates. The discrepancy may be due to an inaccurate surface layer thickness, using half-order kinetics at these high temperatures, and/or neglecting oxidant diffusion within the graphite rod.

For the experiments with pure steam, we assume that P_s is 1 atmosphere. Then the burn-off rate can be calculated from Eqs. (2) and (33) and is independent of the flow rate. The calculated results are given in Table 7. The experiments do however show some dependency on the flow rate, but not nearly as much as that for reaction with oxygen. Nonetheless, the agreement between the calculated and measured burn-off rate is roughly within an order of magnitude.

Table 7. Combustion rate of burning graphite in stagnation flow.

Data Set	Oxidant	graphite ρ and d (g/cm^3), cm	Temp (K)	4V/d (s^{-1})	P_S(est) (atm)	$\dot{m}$ (expt) $Kg/(m^2\ s)$	$\dot{m}$ (calc) $kg/(m^2\ s)$	Source
1	air, 323 K	1.69, 0.5	1200	200	0.040	0.5×10^{-3}	1.3×10^{-3}	Makino 1990
2	air, 323 K	1.69, 0.5	2000	200	0.000007	8×10^{-3}	6.4×10^{-3}	Makino 1990
3	air, 323 K	1.69, 0.5	1200	800	0.083	1×10^{-3}	1.8×10^{-3}	Makino 1990
4	air, 323 K	1.69, 0.5	2000	800	0.000007	60×10^{-3}	6.4×10^{-3}	Makino 1990
5	steam, 370 K	1.82, 1.0	1200	200	1	1×10^{-3}	1×10^{-4}	Makino, et al. 1998
6	steam, 370 K	1.82, 1.0	1900	200	1	13×10^{-3}	7.4×10^{-3}	Makino, et al. 1998
7	steam, 370 K	1.82, 1.0	1200	600	1	1×10^{-3}	1×10^{-4}	Makino, et al. 1998
8	steam, 370 K	1.82, 1.0	1900	600	1	3×10^{-3}	7.4×10^{-3}	Makino, et al. 1998
9	steam, 370 K	1.25, 1.0	1600	50	1	3×10^{-3}	1×10^{-3}	Makino, et al. 1998

10	steam, 370 K	1.25, 1.0	1900	50	1	5×10^{-3}	5×10^{-3}	Makino, et al. 1998
11	steam, 370 K	1.25, 1.0	1200	200	1	1×10^{-3}	7×10^{-5}	Makino, et al. 1998
12	steam, 370 K	1.25, 1.0	1900	200	1	18×10^{-3}	5×10^{-3}	Makino, et al. 1998
13	steam, 370 K	1.25, 1.0	1200	600	1	1×10^{-3}	7×10^{-5}	Makino, et al. 1998
14	Steam, 370 K	1.25, 1.0	1900	600	1	28×10^{-3}	5×10^{-3}	Makino, et al. 1998

11. CONCLUSIONS

The data available for graphite combustion are limited, but nonetheless adequate for an initial assessment of models of this process for use in control volume codes. A simple Arrhenius expression has been used to model the complex reactions of coal combustion, and has also been effectively used to model the simpler system of graphite combustion. Comparisons of the MELCOR default Arrhenius parameters show good agreement with the experimentally obtained parameters.

The coupling of chemical reactions and mass transfer can be readily modeled and analytically solved for simple geometries with integer reaction orders with respect to the oxidant. Numerical solutions are however required for fractional reaction orders even in simple geometries. Dimensionless criteria are derived in this work to determine when mass transfer in either the pore space or the bulk needs to be considered regardless of the reaction order. When pore space diffusion is included and the reaction order is non-integer, the graphs presented in this work may be used to obtain the overall reaction rate. Comparison of the analysis in this work with one set of measurements of coupled diffusion and oxidation showed surprisingly good agreement. The agreement of the model with the surface burn-off experimental data is typically within an order of magnitude, which may be adequate for control volume analysis. Additional measurements of coupled chemical reaction and mass transfer are needed to validate the model for more complex geometries and a variety of oxidants.

12. REFERENCES

Backreedy, R., J. M. Jones, M. Pourkashanian, and A. Williams, "A Study of the Reaction of Oxygen with Graphite: Model Chemistry," *Faraday Discussion*, **119**, 385-394, 2001.

Bews, I. M., A. N. Hayhurst, S. M. Richardson, and S. G. Taylor, "The Order, Arrhenius Parameters, and Mechanism of the Reaction Between Gaseous Oxygen and Solid Carbon," *Combustion and Flame*, **124**, 231-245, 2001.

Bird, R. B., W. E. Stewart, and E. N. Lightfoot, Transport Phenomena, Wiley, New York, 1960.

Bunnell, L. R., T. K. Campbell, and G. L. Tingey, "Oxidation of TSX Graphite Over The Temperature Range 450 to 1200 °C," UNI-3697, UNC Nuclear Industries, Richland, WA, March 1987.

Chelliah, H. K., "The Influence of Heterogeneous Kinetics and Thermal Radiation on the Oxidation of Graphite Particles," *Combustion and Flame*, **104**, 81-94, 1996

Chelliah, H. K., A. Makino, I. Kato, N. Araki, and C. K. Law, "Modeling of Graphite Oxidation in a Stagnation-Point Flow Field Using Detailed Homogeneous and Semiglobal Heterogeneous Mechanisms with Comparisons to Experiments," *Combustion and Flame*, **104**, 469-480, 1996.

Chelliah, H. K. and F. J. Miller, "Heterogeneous Combustion of Porous Graphite Particles in Microgravity," 4th International Microgravity Combustion Workshop, 511-516, University of Virginia, Charlottesville, Virginia, May 1997.

Cole, R. K. and S. B. Rodriguez, "Modification of MELCOR 1.8.4 for Russian Production Reactor Applications- Phases I Through V," Sandia National Laboratories, Albuquerque, New Mexico, January 2000. (Internal Report).

Dahl, R. E., "Oxidation of Reactor Graphite Under High Temperature Reactor Conditions," USAEC report HW-68493, July, 1961.

Eckert, E. R. G. and R. M. Drake, Analysis of Heat and Mass Transfer, McGraw-Hill, New York, 1972.

Froberg R. W. and R. Essenhigh, "Reaction Order and Activation Energy of Carbon Oxidation During Internal Burning," *17th Symposium (International) on Combustion*, Pittsburgh, PA, pp. 179-187, 1978.

Kakac, S., R. K. Shah, and W. Aung, Handbook of Single-Phase Convective Heat Transfer, Wiley and Sons, New York, 1987.

Makino, A. and C. K. Law, "Ignition and Extinction of CO Flame over a Carbon Rod," *Combustion Science and Technology*, **73**, 589-615, 1990.

Makino, A., "A Theoretical and Experimental Study of Carbon Combustion in Stagnation Flow," *Combustion and Flame*, **81**, 166-187, 1990.

Makino, A., N. Araki, and Y. Mihara, "Combustion of Artificial Graphite in Stagnation Flow: Estimation of Global Kinetic Parameters from Experimental Results," *Combustion and Flame*, **96**, 261-274, 1994.

Makino, A., H. Fujizaki, and N. Araki, "Combustion Rate of Burning Graphite in a Stagnation Flow of Water Vapor," *Combustion and Flame*, **113**, 258-263, 1998.

Press, W. H., S. A. Teukolsky, W. T. Vetterling, and B. P. Flannery, Numerical Recipes 2nd Edition, Cambridge University Press, New York, 1992.

Richards, M. B., A. W. Barsell, W. J. Quapp, and M. G. Stamatelatos, "A Computational Model for Graphite Oxidation Under Nuclear Reactor Accident Conditions," *24th National Heat Transfer Conference and Exhibition*, Pittsburgh, PA, American Institute of Chemical Engineers Symposium Series, No. 257, pp. 363-368, 1987.

Schweitzer, D. G. and R. M. Singer, "Oxidation and Heat Transfer Studies in Graphite Channels III. The Chemical Reactivity of BNL Graphite and Its Effect on the Length of Channel Cooled by Air," *Nuclear Science and Engineering*, **12**, 51-58, 1962.

Wichner, R. P. and S. J. Ball, "Potential Damage to Gas-Cooled Graphite Reactors Due to Severe Accidents," Oak Ridge National Laboratories, Oak Ridge, TN, ORNL/TM-13661, April, 1999.

ELECTRONIC DISTRIBUTION

2 Alan Notafrancesco
1 Richard Lee
1 John Jolicoeur
1 Sud Basu
1 Joe Kelly
1 Hossein Esmaili
Mail Stop C3A07M
U.S. Nuclear Regulatory Commission
Washington, DC 20555

1	MS0701	S. M. Gutierrez	6700
1	MS0736	J. E. Kelly	6770
1	MS0736	D. A. Powers	6770
1	MS0748	R. O. Gauntt	6762
1	MS0748	N. E. Bixler	6762
1	MS0748	R. K. Cole	6762
5	MS0748	I. Khalil	6762
1	MS0748	L. L. Humphries	6762
1	MS0748	M. F. Young	6762
1	MS0748	S. B. Rodriguez	6763
1	MS0406	T. O. Townsend	5713
5	MS0406	F. Gelbard	5713

1	MS0899	Technical Library	9536 (electronic copy)


Sandia National Laboratories